Journal of Medicinal Chemistry

Article

pubs.acs.org/jmc

Discovery of 1,2,4-Triazine Derivatives as Adenosine A_{2A} Antagonists using Structure Based Drug Design

Miles Congreve,* Stephen P. Andrews, Andrew S. Doré, Kaspar Hollenstein, Edward Hurrell, Christopher J. Langmead, Jonathan S. Mason, Irene W. Ng, Benjamin Tehan, Andrei Zhukov, Malcolm Weir, and Fiona H. Marshall

Heptares Therapeutics Limited, BioPark, Broadwater Road, Welwyn Garden City, Hertfordshire AL7 3AX, U.K.

Supporting Information

ABSTRACT: Potent, ligand efficient, selective, and orally efficacious 1,2,4-triazine derivatives have been identified using structure based drug design approaches as antagonists of the adenosine A_{2A} receptor. The X-ray crystal structures of compounds **4e** and **4g** bound to the GPCR illustrate that the molecules bind deeply inside the orthosteric binding cavity. In vivo pharmacokinetic and efficacy data for compound **4k** are presented, demonstrating the potential of this series of compounds for the treatment of Parkinson's disease.

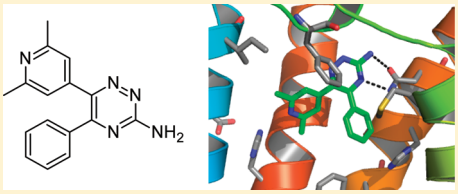

INTRODUCTION

The adenosine A_{2A} receptor is expressed in the basal ganglia where it functionally opposes the actions of the dopamine D_2 receptor, i.e., inhibition of the A_{2A} receptor leads to enhancement of D_2 receptor function. Given that the primary pathology in Parkinson's disease is a loss of nigrostriatal dopamine and hence reduced dopamine D_2 receptor activation, adenosine A_{2A} receptor antagonism has emerged as a potential nondopaminergic therapy for this disorder. Preclinically, adenosine A_{2A} receptor antagonists are effective in animal models of Parkinson's disease, ranging from the reversal of haloperidol-induced catalepsy through to efficacy in more disease-relevant models such as 6-hydroxydopamine lesioned rats and MPTP-lesioned primates.[1] Furthermore, a number of these compounds have progressed into clinical development, the most advanced of which is currently preladenant. This compound was shown to be effective in a phase IIa trial of patients with moderate-to-severe Parkinson's disease when administered in conjunction with levodopa, increasing on-time with no concomitant increase in dyskinesias.[2]

In the preceding publication, hit molecules derived from a virtual screening strategy were described.[3] One series of 1,3,5-triazine derivatives was identified and optimized to give potent and selective adenosine A_{2A} receptor antagonists. As part of the optimization of this chemotype and by considering the proposed binding mode to the receptor, we hypothesized that the alternative 1,2,4-triazine isomers might also bind to the receptor but could sit more deeply in the receptor pocket accessing the region normally occupied by the ribose group of the natural ligand adenosine, in addition to mimicking the adenine ring itself. Upon testing of the commercially available parent 5,6-diphenyl-1,2,4-triazine-3-amine **4a**, we discovered that the molecule was indeed an antagonist of the receptor (Table 1, compound **1**; $pK_i = 6.93$). In this paper, we outline our studies in this isomeric chemical series.

RESULTS AND DISCUSSION

Design and Synthesis. The binding mode of 1,2,4-triazine derivatives was initially derived from modeling of representative compounds in an "experimentally enhanced" homology model of the adenosine A_{2A} receptor (described in the preceding paper), refined using site directed mutagenesis data both from the literature and our own Biophysical Mapping (BPM) approach.[3−6] Parts A and B of Figure 1 illustrate the proposed binding mode of two analogues **4g** and **4e** (Table 1) in the orthosteric binding site of the receptor and also show the BPM binding fingerprint around these example ligands, used to refine and improve the model. The residues that, when mutated to alanine, reduce binding of each ligand are colored in red for nonbinding, dark-orange for the largest effect (tier 1), orange for the next largest effect (tier 2), yellow for the smallest effect (tier 3), and in green if the mutation caused an increase in binding of the ligand. The BPM studies have been reported elsewhere and analogues **4e** and **4g** here equate to examples **3b** and **3d** in the earlier publication.[4] As well as rationalizing the role of the aminoheterocyclic scaffold binding to Asn253$^{6.55}$ (superscripts refer to Ballesteros−Weinstein numbering),[7] in particular the BPM fingerprints and modeling suggested that presence of a hydrogen bond acceptor at the para position of ring A of the ligands to His278$^{7.43}$ with addition of one or more flanking lipophilic substituents on the same ring to interact with Ile66$^{2.64}$ and Ser277$^{7.42}$ should be one focus of the SAR program (R^1, R^2, R^3 positions in Scheme 1 and Table 1). In addition, careful 3D analysis of the GRID maps, calculated for both A_{2A} and an A_1 homology model, enabled the pharmacophoric preferences (hydrophobic, hydrogen-bond donor and acceptor) and shape constrictions/differences to be identified to allow an enhanced evaluation of each ligand

Received: October 12, 2011
Published: January 5, 2012

Table 1. SAR and in Vitro ADME Data for Compounds 4a to 4l[a]

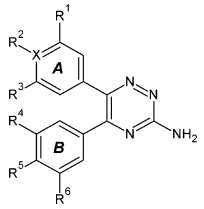

ID	formula	A_{2A} pK_i	A_1 pK_i	LE[17]	RLM (min)	PPB (%)	kinetic solubility (μM)	SPR data			
								k_a	k_d	K_D	pK_D
4a	X=C; R^{1-6}=H	6.93	6.56	0.50	23	ND	>100	>5 × 10^7	>1 × 10^0	9.03 × 10^{-6}	5.0
4b	X=C; R^1=Cl; R^{2-6}=H	7.29	7.25	0.50	29	97.9	13	3.79 × 10^5	1.68 × 10^{-1}	4.42 × 10^{-7}	6.4
4c	X=C; R^1=R^3=Cl; $R^{2,4,5,6}$ =H	8.40	7.36	0.55	108	99.0	38	5.32 × 10^5	2.43 × 10^{-2}	4.57 × 10^{-8}	7.3
4d	X=C; R^1=R^3=Me; $R^{2,4,5,6}$=H	7.67	6.71	0.50	9	98.0	20	ND	ND	ND	ND
4e	X=C; R^1=Cl; R^3=OH; $R^{3,4,5,6}$ =H	8.85	9.79	0.57	69	98.0	45	4.07 × 10^6	1.01 × 10^{-3}	2.48 × 10^{-10}	9.6
4f	X=C; R^1=R^3=Me; R^2=OH; $R^{4,5,6}$=H	8.39	7.78	0.52	75	93.3	43	8.57 × 10^6	1.36 × 10^{-3}	1.59 × 10^{-10}	9.8
4g	X=N; R^1=R^3=Me; $R^{4,5,6}$=H	8.11	7.07	0.53	100	82.1	40	9.92 × 10^6	1.15 × 10^{-2}	1.16 × 10^{-9}	8.9
4h	X=N; R^1=R^3=Me; R^5=F; $R^{4,6}$=H	7.81	6.40	0.48	100	69.0	43	1.13 × 10^7	1.15 × 10^{-1}	1.02 × 10^{-8}	8.0
4i	X=N; R^1=R^3=Me; $R^{4,6}$=F; R^5=H	7.56	6.77	0.45	100	ND	45	9.44 × 10^6	8.84 × 10^{-2}	9.37 × 10^{-9}	8.0
4j	X=N; R^1=R^3=Me; R^4=F; $R^{5,6}$=H	7.98	6.96	0.49	78	87.0	48	1.41 × 10^7	4.27 × 10^{-2}	3.03 × 10^{-9}	8.5
4k	X=N; R^1=Me; R^3=CF_3; $R^{4,5,6}$=H	8.46	7.50	0.48	86	92.0	35	1.08 × 10^6	3.73 × 10^{-3}	3.45 × 10^{-9}	8.5
4l	X=N; R^1=Me; R^3=CF_3; R^5=F; $R^{4,6}$=H	8.34	6.93	0.45	97	93.0	34	1.55 × 10^6	4.09 × 10^{-2}	2.63 × 10^{-8}	7.6

[a]RLM rat liver microsome half-life in mins; PPB rat plasma protein binding; SPR kinetics using A_{2A}–StaR (see main text).

docked into the binding site.[8,9] Very subtle binding site differences, such as A_{2A}–Ser$^{7.42}$ to A_1–Thr$^{7.42}$ and A_{2A}–Ala$^{2.57}$ to A_1–Val$^{2.57}$ and also ligand preferences between the two receptor models were exploited to overall enable the design of small, polar, selective, and ligand-efficient compounds.

During the SAR optimization process, a number of members of the series were successfully cocrystallized in the receptor using the published thermally stabilized adenosine A_{2A} construct A_{2A}–StaR2 (stabilized receptor or StaR) developed in our laboratories.[10] This allowed, for the first time to our knowledge, X-ray structure-directed optimization of a hit series to derive potent and selective leads for a G protein-coupled receptor. This reinforced our efforts focused on the optimization of the substitution patterns around the pendent aryl rings A and B in an atom efficient manner (Scheme 1 and Table 1) to engineer high potency and reduce affinity for the adenosine A_1 receptor without significantly increasing molecular weight or lipophilicity. The X-ray structures also validated the BPM approach, which had successfully predicted the binding mode of the compounds but add a further level of understanding particularly with respect to teasing out selectivity for A_{2A} over the A_1 receptor.

Synthesis of the target compounds began with a set of purchased 3-amino-5-aryl-1,2,4-triazine derivatives **1**, Scheme 1. These building blocks were further elaborated following treatment with NBS at room temperature to afford the corresponding 6-bromotriazines **2**. A set of conditions was optimized to enable Suzuki cross-coupling of a diverse range of bromotriazines with commercially available boronic acid derivatives. Thus **2** and **3** were coupled at 150 °C in a sealed vessel in the presence of catalytic quantities of $Pd(PPh_3)_4$ to afford the biaryl triazines of interest (**4**). Access to bespoke 4-pyridylboronic acid derivatives was required to synthesize molecules suggested by the proposed binding mode in the receptor. Using a method described by Hartwig et al., commercial 2,6-disubstituted pyridines **5** were borylated in high yield, under iridium catalysis, with bis(pinacolato)-diboron.[11−13]

X-Ray Crystallography. The overall structure of the A_{2A}–StaR2 in complex with compounds **4e** and **4g** is in close agreement to the previously solved structures in our laboratory and methods for crystallization and a description of the general receptor architecture are described elsewhere.[10] Statistics for data collection and refinement are given in Supporting Information Table S1. The cocrystal structures of the A_{2A}–StaR2 in complex with compounds **4g** and **4e** (Figure 1C,D) show clear positive omit density at 3.0σ (data not shown) for the presence and position of the ligands in the receptor binding pocket. The structure of A_{2A}–StaR2–**4g** shows the amino-triazine core makes two critical donor and acceptor H-bonding interactions with the side chain of Asn253$^{6.55}$ with bonding distances of 2.85 and 2.76 Å, respectively. In addition, the helical portion of extracellular loop (ECL) 2 is positioned for Phe168 to form a perpendicular $\pi-\pi$ stack on one side of the core, while the side chain of Met270$^{7.35}$ makes a hydrophobic interaction on the opposite side, completing the receptor interactions around this region of the ligand. The phenyl substituent from the C5 position of the triazine core occupies a hydrophobic pocket deeper inside the receptor flanked by Leu84$^{3.32}$, Leu85$^{3.33}$, Met177$^{5.38}$, Asn181$^{5.42}$, Trp246$^{6.48}$, Leu249$^{6.51}$, and His250$^{6.52}$. The second substituent, dimethyl-pyridine, from the C6 carbon of the triazine core occupies the ribose binding pocket (of the natural agonist adenosine) defined by His278$^{7.43}$ and Ser277$^{7.42}$, with one methyl substituent pointing toward a hydrophobic region defined by Ala63$^{2.61}$ and Ile66$^{2.64}$ and the other pointing toward the stabilizing mutation Ser277$^{7.42}$Ala.[14] Additionally, the side chain of His278$^{7.43}$ is positioned 4.03 Å away from N4 of the dimethyl-pyridine substituent, precluding a direct H-bond between the ligand and this receptor residue. Compound **4e** occupies a similar position overall to that of **4g** in the A_{2A} receptor ligand binding site but with specific differences. The

dx.doi.org/10.1021/jm201376w | J. Med. Chem. 2012, 55, 1898−1903

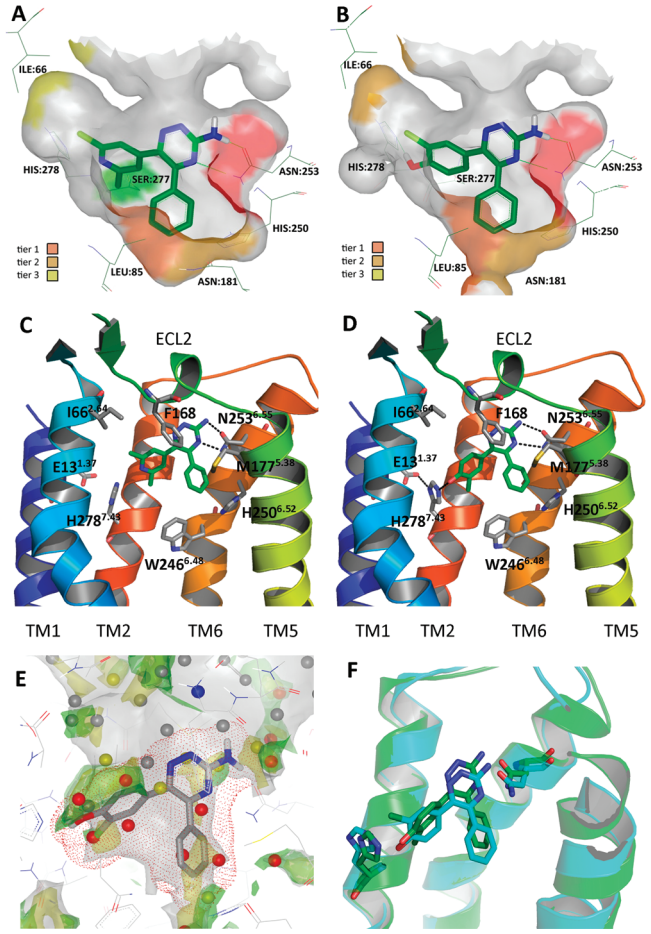

Figure 1. (A,B) BPM fingerprint of 1,2,4-triazine adenosine A_{2A} antagonists. Compounds **4g** (A) and **4e** (B) are illustrated bound to the orthosteric pocket of the receptor and the residues lining the pocket that interact with the ligands are labeled. The tier 1, 2, and 3 designation is described in the main text. The key hydrogen bonding to Asn253$^{6.55}$ of the scaffold is highlighted by green dotted lines. (C,D) Illustration of the A_{2A}–StaR2 ligand binding site in complex with compound **4g** (C) and **4e** (D). TM helices and visible extracellular regions are depicted in the rainbow format. Ligands are represented as stick models, carbon and chlorine atoms are green, oxygen atoms red, and nitrogen atoms blue. Residues involved in ligand binding are labeled and represented as gray sticks, oxygen atoms are red, and nitrogen atoms are blue. Extracellular loop 2, the key binding site residues and TM's 1, 2, 5, and 6 are labeled for reference. Potential H-bonds between the ligand and receptor are represented as dashed blue lines. TM3 and TM4 have been omitted for clarity. (E) WaterMap calculation on the binding site of compound **4e** (ligand removed for the calculation). Waters calculated are color coded to show the most "unhappy" vs bulk solvent as red (>3.5 kcal/mol), then yellow (2.2–3.5 kcal/mol), with gray intermediate (−1 to 2.2 kcal) and blue "happy" (<−1 kcal/mol). The CPK surface of the ligand **4e** is shown as a red dot surface, clearly illustrating that the cluster of red and yellow "unhappy" waters deep in the binding site have been displaced. GRID maps are also shown that highlight the shape (Csp3 (C3) at 1 kcal/mol in light-gray), the lipophilic hotspots (aromatic CH probe (C1═) in yellow at −2.5 kcal/mol), and the water probe hotspots (in green wire mesh at −6.6 kcal/mol). (F) Alignment of the A_{2A} homology model with **4e** docked (cyan carbons) onto the crystal structure of A_{2A}–**4e** complex (green carbons). The alignment was generated by the align algorithm in Pymol utilizing only helices where hydrogen bonds are formed with the ligand, helices 6 and 7. Helices 2, 3, and 4 are removed for clarity.

amino-triazine core makes a similar set of interactions to the receptor as **4g**, however, the bond lengths to Asn253$^{6.55}$ increase to 3.12 and 3.1 Å in comparison. The driving force for this is an additional hydrogen bond, 2.87 Å in length, formed between the phenolic hydroxyl on the chloro-phenol substituent to Nε of His278$^{7.43}$. Additionally, Glu13$^{1.37}$ has switched rotamer and is now poised to H-bond to Nδ1 of His278$^{7.43}$. The additional conjugation of the ligand through the receptor pulls compound **4e** ~1.2 Å deeper into the ribose binding pocket in comparison to **4g** (pivoting on the common phenyl group) and perhaps provides a basis for the slow off-rate receptor kinetics of these phenolic compounds (see Table 1). It is noted that two potential conformations for the phenyl and dimethyl-pyridine substituents (compound **4g**), and the phenyl and chloro-phenol substituents (compound **4e**), involving concomitant ~50° rotations of each around the bond to the amino-triazine core, can exist in nature. In the structures presented here the conformations with the lower *b*-factors were submitted to the Research Collaboratory for Structural Bioinformatics Protein Data Bank (RCSB).

An analysis of the A_{2A} binding site (with ligand **4e** removed) using the WaterMap software (Schrödinger)[15] shows that these highly ligand efficient ligands (LE = 0.57 for **4e**) occupy exactly the region where there is a cluster of "unhappy" waters (shown as red and yellow balls in Figure 1E) and not other less favorable regions (as for example less ligand efficient compounds such as ZM241385 bind, reported elsewhere).[16] The WaterMap software uses a molecular dynamics simulation on a full explicit water network to calculate the enthalpic and entropic energies of waters compared to bulk solvent. Finally, in Figure 1, as the initial SAR work was based on our BPM-optimized homology model, we include a comparison of a docked structure of **4e** into the homology model and the protein–ligand X-ray structure, showing that the overall orientation and key hydrogen bond interactions were correctly predicted (Figure 1f). The biophysical mapping fingerprints of compounds **4e** and **4g** (published previously by Zhukov et al, as compounds **3b** and **3d** in Table 1), respectively, are in excellent agreement with the crystal structures, highlighting the significant interactions with Ile66$^{2.64}$, Leu85$^{3.33}$, Asn181$^{5.42}$, and Asn253$^{6.55}$ and confirming the initial deep placement of the ligand in the ribose sugar pocket of the A_{2A} receptor.[4]

Structure–Activity Relationship. The parent compound **4a** was identified as a ligand efficient adenosine A_{2A} receptor antagonist (Table 1).[17] Having examined the putative binding mode in silico, SAR focused on simple substitution of rings A and B (Table 1). During the optimization process, the binding mode predictions were first improved using our BPM approach and then by determination of the crystal structures of compounds **4e** and **4g** (discussed above). The models suggested only small groups would be tolerated, particularly in ring B, and this was quickly evident because addition of chlorine or methyl in ring A and fluorine in ring B was tolerated or increased affinity (compounds **4a–d** and **4h–j**), but larger groups tended to be detrimental to potency (data not shown). The models also suggested the potential to form hydrogen bonding interactions from ring A at the para position R^2, and introduction of either a phenolic hydroxyl (compounds **4e** and **4f**) or a 4-pyridyl nitrogen (compound **4g**) were found to increase potency (compare **4f** and **4g** with **4d**). A challenging aspect of the optimization was that affinity for the adenosine A_1 receptor was generally also observed, and it was thought desirable to reduce affinity against this target to avoid any

dx.doi.org/10.1021/jm201376w | J. Med. Chem. 2012, 55, 1898–1903

Scheme 1. Synthesis of 5,6-Biaryl-1,2,4-triazine-3-amine Derivatives (4) and 4-Pyridylboronic Acid Derivatives (6)[a]

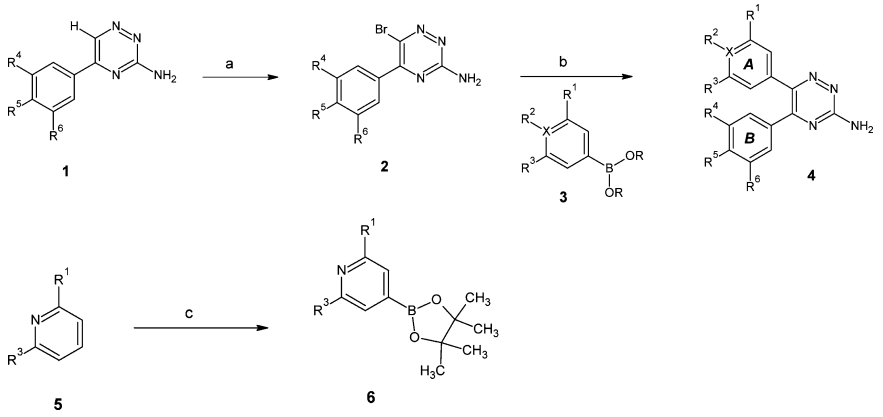

[a]Reagents and conditions: (a) NBS, DMF, RT; (b) **3**, $Pd(PPh_3)_4$, K_2CO_3, 1,4-dioxane/H_2O, 150 °C; (c) $[Ir(COD)OMe]_2$, DTBPY, $[B(pin)]_2$, hexane, 50 °C.

potential side effects caused by cross reactivity with this receptor. It was quickly noted, consistent with small differences in the binding sites predicted from a GRID analysis of models of the two receptors (discussed above), that 3,5-disubstitution in ring A introduced a modest selectivity for A_{2A} over A_1 (compare **4b** with **4c** and **4e** with **4f**). Also, although a very subtle effect, introduction of fluorine at R^5 on ring B reduced activity against both receptors but slightly improved the selectivity window for A_{2A} over A_1 (compare **4g** with **4h**). Introduction of fluorine in other substitution patterns tended to reduce affinity further or had no additional selectivity benefit (compounds **4i** and **4j**). Overall, the derivatives were found to be highly selective over the adenosine A_3 receptor, e.g., compounds **4c**, **4g**, and **4h** had antagonist affinity of >10 μM. The series was generally 10-fold selective over the A_{2B} subtype, and inhibition of this target was not thought to be detrimental therapeutically; **4c**, **4g**, and **4h** had pK_i values of 7.4, 7.3, and 6.8, respectively (A_3 and A_{2B} data were generated by Ricerca Biosciences, Taipei). Fine tuning of affinity by various combinations of small lipophilic substituents quickly led us to pyridyl analogues **4k** and **4l**, incorporating a CF_3 group at the 3-position of ring A with methyl at the 5-position and with or without fluorine at the para position of ring B. These two compounds have the best balance of potency and selectivity, derived by introduction of simple substituents on the scaffold, of the examples shown in the Table.

Table 1 also details the binding kinetics of compounds from the lead series as measured using the adenosine A_{2A}–StaR by surface plasmon resonance on a Biacore instrument (see Supporting Information for full details). The pK_D values were generally in good agreement with the radioligand binding data, and the method also allowed comparison of on rates (k_a) and off rates (k_d) to the receptor between related compounds. Of most note in the data presented here is that the phenolic analogues **4e** and **4f** had very slow off rates, consistent with the change in binding mode observed in the crystal structure of **4e** discussed above. Consideration of relative receptor kinetics was part of the decision making process used for selection of compounds for in vivo efficacy experiments.

Pharmacokinetics and in Vivo Efficacy. The examples in Table 1 generally exhibited good physicochemical and in vitro ADME properties, having moderate to high aqueous solubility, good stability in rat liver microsomes (RLM) and, where a polar substituent had been introduced (such as a pyridyl nitrogen atom), relatively low plasma protein binding (PPB). Another general trend was a lack of inhibition of cytochrome P450 enzymes and the hERG channel, with only the occasional outlier (data not shown). A number of compounds also demonstrated good pharmacokinetic properties in rat dosed either orally or intravenously. Data is given here for example **4k** in a rat pharmacokinetic (PK) experiment; PK parameters are shown in Table 2. Compound **4k** displayed moderate clearance

Table 2. PK Parameters of Compound 4k in Rat

4k, 1 mg/kg (IV)		**4k**, 2 mg/kg (PO)	
plasma clearance	42 mL/min/kg	T_{max}	0.4 h
V_d (ss)	4.6 L/kg	C_{max}	244 ng/mL
terminal $t_{1/2}$	1.2 h	terminal $t_{1/2}$	1.1 h
AUC_{inf}	397 ng·h/mL	AUC_{inf}	846 ng·h/mL
brain:plasma (0.5 h)	3.2	F_{po}	100%
CSF:brain (0.5 h)	0.036		

(42 mL/min/kg), although due to a relatively high steady-state volume of 4.6 L/kg, the compound had an acceptable half-life of 1.2 h. Compound **4k** was rapidly absorbed after oral dosing (T_{max} = 0.4 h) and displayed good exposure with AUC = 846 ng·h/mL, resulting in an estimated F_{po} of 100%. The derivative also displayed excellent brain penetration, as measured by samples at 0.5 h post-IV dose (brain/plasma = 3.2). Furthermore, measured levels in the CSF at the same time point suggested that the unbound fraction of **4k** in the brain was 3.6%, reasonably consistent with the measured plasma protein binding in vitro of 92% (unbound plasma fraction = 8%).

Given the good overall in vitro ADME and in vivo PK profile of **4k**, especially with respect to brain penetration and oral bioavailability, the compound was tested for its ability to reverse haloperidol-induced catalepsy in rats, a simple and well validated in vivo pharmacodynamic model mimicking the loss of striatal dopamine receptor function observed in Parkinson's disease.[1] Compound **4k** was found to very potently reverse catalepsy induced by haloperidol, with ED_{50} values of 0.2 mg/kg at both 1 and 2 h post dose time points (Figure 2).

CONCLUSIONS

The studies presented here have shown for the first time that biophysical mapping and cocrystal X-ray structures of ligands to

dx.doi.org/10.1021/jm201376w | J. Med. Chem. 2012, 55, 1898–1903

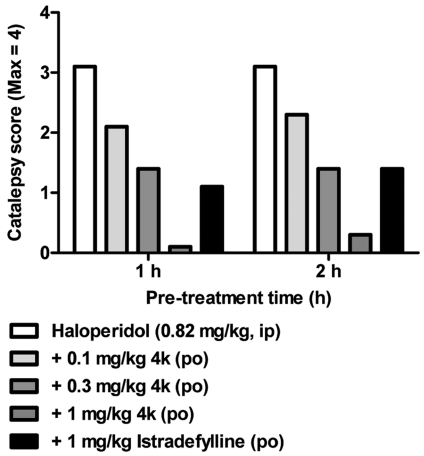

Figure 2. In vivo efficacy of **4k**. Dose-dependent effect of **4k** (0.1−1 mg/kg, po; 1 and 2 h pretreatment time) to reverse haloperidol-induced catalepsy in rats in comparison with the positive control, istradefylline (1 mg/kg, po).

a G protein-coupled receptor can be used to direct optimization of novel, low molecular weight hit molecules into highly potent and selective lead compounds. Compound **4k**, described above, has desirable physicochemical and drug-like properties, including high oral bioavailability and very potent in vivo efficacy. Further optimization of this 1,2,4-triazine series of antagonists of the adenosine A_{2A} receptor has subsequently allowed identification of a preclinical candidate for the potential treatment of Parkinson's disease, and details of the development of this molecule will be the topic of future publications.

EXPERIMENTAL SECTION

Synthetic Methods. The purity of the final compounds was determined by HPLC or LC/MS analysis to be >95%. Full experimental details of all compounds in Table 1 are described in the Supporting Information. Synthesis of compounds **4g** and **4k** are described below.

6-Bromo-5-phenyl-1,2,4-triazin-3-amine. A solution of 5-phenyl-1,2,4-triazin-3-amine (1.50 g, 8.70 mmol) in DMF (15 mL) was cooled to −25 °C and treated with a solution of *N*-bromosuccinimide (4.50 g, 26.6 mmol) in DMF (10 mL) by dropwise addition. The reaction was warmed gradually to room temperature and stirred overnight with TLC monitoring. After completion of the reaction, the mixture was poured into saturated bicarbonate solution (50 mL) and extracted with diethyl ether (25 × 3 mL). The organic phases were combined, dried over Na_2SO_4, and concentrated in vacuo. The crude compound was purified by gradient flash chromatography, eluting with mixtures of ethyl acetate in hexane to afford 6-bromo-5-phenyl-1,2,4-triazin-3-amine (1.40 g, 64%). HPLC: 99%, 8.31 min (244 nm). Mass spectroscopy: m/z 250.9 $[M + H]^+$. ^1H NMR: (400 MHz, DMSO) δ: 7.49−7.57 (m, 5H), 7.72 (m, 2H).

2-(Trifluoromethyl)-4-(4,4,5,5-tetramethyl-1,3,2-dioxaborolan-2-yl)-6-methylpyridine. Methoxy(cyclooctadiene)iridium(I) dimer (30 mg, 0.062 mmol), 4,4′-di-*tert*-butyl-2,2′-bipyridine (33 mg, 0.124 mmol), and bis(pinacolato)diboron (4.09 g, 16.1 mmol) were added to a flask which had been thoroughly purged with nitrogen. The flask was once more purged before adding hexane via syringe (30 mL). The resulting mixture was heated at 50 °C for 10 min until the appearance of a dark-red solution was observed. 2-Trifluoromethyl-6-methyl pyridine (4.0 g, 24.8 mmol) was then added by syringe, and heating continued for a further 6 h. After cooling to room temperature, the crude reaction mixture was concentrated under reduced pressure. The resulting residue was purified by column chromatography, eluting with ethyl acetate/hexane mixtures to afford the target compound 2-(trifluoromethyl)-4-(4,4,5,5-tetramethyl-1,3,2-dioxaborolan-2-yl)-6-methylpyridine (5.9 g, 83%). HPLC: 96%, 7.57 min (210 nm). Mass spectroscopy: m/z 287.8 $[M + H]^+$. ^1H NMR: (400 MHz, DMSO) δ: 1.31 (s, 12 H), 2.51 (s, 3H), 7.70 (s, 1H), 7.76 (s, 1H).

6-(2,6-Dimethylpyridin-4-yl)-5-phenyl-1,2,4-triazin-3-amine ***4g****: A Typical Procedure for the Synthesis of 5,6-Biaryl-1,2,4-triazine-3-amine derivatives.* A solution of 6-bromo-5-phenyl-1,2,4-triazin-3-amine, (90 mg, 0.358 mmol) in dioxane (2.0 mL) was treated with 2,6-dimethyl-4-(4,4,5,5-tetramethyl-1,3,2-dioxaborolan-2-yl)pyridine (96 mg, 0.412 mmol) and K_2CO_3 (148 mg, 1.07 mmol). The resulting mixture was diluted with water (1.0 mL), degassed, treated with tetrakis triphenylphosphinepalladium(0) (21 mg, 0.018 mmol), and stirred for 2 h at 150 °C in a sealed vessel. Upon completion of the reaction, the mixture was diluted with water (20 mL) and extracted with ethyl acetate (3 × 20 mL); the combined organic extracts were then dried over Na_2SO_4 and concentrated under reduced pressure. The crude compound was purified by gradient flash chromatography, eluting with mixtures of ethyl acetate and hexanes to afford 6-(2,6-dimethylpyridin-4-yl)-5-phenyl-1,2,4-triazin-3-amine **4g** (44 mg, 43%). HPLC: 98%, 6.09 min (281 nm). Mass spectroscopy: m/z 278.1 $[M + H]^+$. ^1H NMR: (400 MHz, DMSO) δ: 2.33 (s, 6H), 6.97 (s, 2H), 7.37−7.43 (m, 4H), 7.48 (m, 1H), 7.58 (bs, 2H).

6-[2-Methyl-6-(trifluoromethyl)pyridin-4-yl]-5-phenyl-1,2,4-triazin-3-amine ***4k****.* 6-[2-Methyl-6-(trifluoromethyl)pyridin-4-yl]-5-phenyl-1,2,4-triazin-3-amine **4k** (0.32 g, 35%) was prepared from 6-bromo-5-phenyl-1,2,4-triazin-3-amine (0.70 g, 2.78 mmol) and 2-methyl-4-(4,4,5,5-tetramethyl-1,3,2-dioxaborolan-2-yl)-6-trifluoromethyl-pyridine (1.2 g, 4.1 mmol) according to the typical procedure described above. HPLC purity: 99%, 10.29 min (269 nm). Mass spectroscopy: m/z 332.0 $[M + H]^+$. ^1H NMR: (400 MHz, DMSO) δ: 2.48 (s, 3H), 7.38 (m, 5H), 7.47 (s, 1H), 7.58 (s, 1H), 7.73 (bs, 2H).

Biology Methods. Methods for determination of antagonist potency against human adenosine A_{2A} and A_1 receptors, binding constants, and receptor kinetics of compounds binding to the A_{2A}−StaR by surface plasmon resonance and the procedure for determination of in vivo efficacy in rodents by reversal of haloperidol induced catalepsy are detailed in the Supporting Information.

Diffraction Data Collection of A_{2A}−StaR2 in Complex with 4e and 4g. Diffraction data from crystals of A_{2A}−StaR2 in complex with compounds **4e** and **4g** were collected at I24, Diamond Light Source, Oxford, UK. Statistics for data collection and refinement are given in Supporting Information Table S1. Atomic coordinates and structure factors have been deposited in the RCSB under accession codes 3UZC and 3UZA, respectively.

Computational Chemistry. Homology models were constructed from the avian β_1 adrenergic GPCR crystal structure bound to cyanopindolol (PDB: 2VT4) using several computational approaches as detailed in the preceding paper and refined/validated using site-directed mutagenesis and BPM data and known ligands (see Supporting Information for full details).[3,4] Docking was done using Glide SP and XP (Schrödinger), and GRID analyses of the binding sites was used to evaluate potential docking poses (using the Csp3 (C3) for shape, aromatic CH probe (C1═) for lipophilic hotspots, carbonyl group (O) for hydrogen-bond acceptor hotspots, and amide NH (N1) for hydrogen-bond donor hotspots) and driving the designs.[8,9]

ASSOCIATED CONTENT

Supporting Information

Crystallographic table of statistics. Synthesis protocols, ^1H NMR, purification details, yields, purities by HPLC and MS or LCMS. Biological protocols for in vitro and in vivo experiments. Computational chemistry methods. SPR binding and kinetic data. This material is available free of charge via the Internet at http://pubs.acs.org.

Accession Codes

The PDB codes for **4g** and **4e** are 3UZA and 3UZC, respectively.

AUTHOR INFORMATION

Corresponding Author

*Phone +44 (0)1707 358638. E-mail: miles.congreve@heptares.com.

ACKNOWLEDGMENTS

We thank Chris Richardson and Bissan Al-Lazikani for help with constructing the first generation of homology models and ligand dockings, David Myszka for helping to establish conditions for use of A_{2A} StaRs on the Biacore format as a precursor to the work in this manuscript, and Nathan Robertson, Asma Baig, Jason Brown, Alistair O'Brien, and Giles Brown at Heptares.

ABBREVIATIONS USED

StaR, stabilized receptor; BPM, biophysical mapping; GPCR, G protein-coupled receptor; SPR, surface plasmon resonance; ECL, extracellular loop; TM, transmembrane helix; SAR, structure−activity relationship; PDB, Protein Data Bank; LE, ligand efficiency; RLM, rat liver microsomal turnover; PPB, rat plasma protein binding; RCSB, Research Collaboratory for Structural Bioinformatics Protein Data Bank

REFERENCES

(1) Shah, U.; Hodgson, R. Recent progress in the discovery of adenosine A_{2A} receptor antagonists for the treatment of Parkinson's disease. *Curr. Opin. Drug Discovery Dev.* **2010**, *13*, 466−480.

(2) Salamone, J. D. Preladenant, a novel adenosine A_{2A} receptor antagonist for the potential treatment of parkinsonism and other disorders. *IDrugs* **2010**, *13*, 723−731.

(3) Langmead, C. J.; Andrews, S.; Congreve, M.; Errey, J.; Hurrell, E.; Marshall, F. H.; Mason, J. S.; Richardson, C.; Robertson, N.; Zhukov, A.; Weir, M. Identification of Novel Adenosine A_{2A} Receptor Antagonists by Virtual Screening. Just accepted. DOI: 10.1021/jm201455y. Published online: January 17, 2012

(4) Zhukov, A.; Andrews, S. P.; Errey, J. C.; Robertson, N.; Tehan, B.; Mason, J. S.; Marshall, F. H.; Weir, M.; Congreve, M. Biophysical Mapping of the Adenosine A_{2A} Receptor. *J. Med. Chem.* **2011**, *54*, 4312−4323.

(5) Dal Ben, D.; Lambertucci, C.; Marucci, G.; Volpini, R.; Cristalli, G. Adenosine Receptor Modeling: What Does the A_{2A} Crystal Structure Tell Us? *Curr. Top. Med. Chem.* **2010**, *93*, 993−1018.

(6) Kim, S. K.; Gao, Z.; Van Rompaey, P.; Gross, A. S.; Chen, A.; Van Calenbergh, S.; Jacobson, K. A. Modeling the adenosine receptors: comparison of the binding domains of A_{2A} agonists and antagonists. *J. Med. Chem.* **2003**, *46*, 4847−4859.

(7) Ballesteros, J. A.; Weinstein, H.; Stuart, C. S. Integrated methods for the construction of three dimensional models and computational probing of structure−function relations in G protein coupled receptors. In *Methods in Neurosciences*; Academic Press: New York, 1995; Vol. *25*, pp 366−428.

(8) Goodford, P. J. A computational procedure for determining energetically favorable binding sites on biologically important macromolecules. *J. Med. Chem.* **1985**, *28*, 849−857.

(9) Sciabola, S.; Stanton, R. V.; Mills, J. E.; Flocco, M. M.; Baroni, M.; Cruciani, G.; Perruccio, F.; Mason, J. S. High-throughput virtual screening of proteins using GRID molecular interaction fields. *J. Chem. Inf. Model.* **2010**, *50*, 155−169.

(10) Doré, A. S.; Robertson, N.; Errey, J. C.; Ng, I.; Hollenstein, K.; Tehan, B.; Hurrell, E.; Bennet, K.; Congreve, M.; Magnani, F.; Tate, C. G.; Weir, M.; Marshall, F. H. Structure of the adenosine A_{2A} receptor in complex with ZM241385 and the xanthines XAC and caffeine. *Structure* **2011**, *19*, 1283−1293.

(11) J. Takagi, J.; Sato, K.; Hartwig, J. F.; Ishiyama, T.; Miyaura, N. Iridium-catalyzed C−H coupling reaction of heteroaromatic compounds with bis(pinacolato)diboron: regioselective synthesis of heteroarylboronates. *Tetrahedron Lett.* **2002**, *43*, 5649−5651.

(12) Murphy, J. M.; Liao, X.; Hartwig., J. F. Meta Halogenation of 1,3-Disubstituted Arenes via Iridium-Catalyzed Arene Borylation. *J. Am. Chem. Soc.* **2007**, *129*, 15434−15435.

(13) Ishiyama, T.; Takagi, J.; Nobuta, Y.; Miyaura., N. Iridium-catalyzed C−H borylation of arenes and heteroarenes: 1-chloro-3-iodo-5-(4,4,5,5-tetramethyl-1,3,2-dioxaborolan-2-yl)benzene and 2-(4,4,5,5,-tetramethyl-1,3,2-dioxaborolan-2-yl)indole. *Org. Synth.* **2005**, *82*, 126−132.

(14) Lebon, G.; Warne, T.; Edwards, P. C.; Bennett, K.; Langmead, C. J.; Leslie, A, G. W.; Tate, C. G. Agonist-bound adenosine A_{2A} receptor structures reveal common features of GPCR activation. *Nature* **2011**, *474*, 521−523.

(15) Higgs, C.; Beuming, T.; Sherman, W. Hydration site thermodynamics explain SARs for triazolylpurines analogues binding to the A_{2A} receptor. *ACS Med. Chem. Lett.* **2010**, *1*, 160−164.

(16) Congreve, M.; Langmead, C. J.; Mason, J. S.; Marshall, F. H. Progress in Structure Based Drug Design for G Protein-Coupled Receptors. *J. Med. Chem.* **2011**, *54*, 4283−4311.

(17) Hopkins, A. L.; Groom, C. R.; Alex, A. Ligand efficiency: a useful metric for lead selection. *Drug Discovery Today* **2004**, *9*, 430−431.